Continuum model for mesh crystallization

Alexander Tetervak, Stephen Hudson, Jizhong Zhang,* and Jeffrey L. Hutter†
Department of Physics and Astronomy, The University of Western Ontario, London, Ontario, Canada N6A 3K7
(Received 18 October 2004; revised manuscript received 18 February 2005; published 17 May 2005)

The front propagation of a single crystallizing domain has been well studied for more than a century. In many important crystallization processes, however, multiple domains grow simultaneously, resulting in a multicrystalline, meshlike aggregate. This is the typical case for organic compounds, including polymers and alkanes. We have studied such growth in the case of a normal alkane precipitating from solution in the presence of kinetic inhibitors—additives which, when present in trace amounts, have a dramatic effect on growth kinetics and morphology. In this case, we observe a distinct banded growth with a typical length scale of 300 μm superimposed on the finer mesh structure. We present a simple continuum model that demonstrates the essential behavior of this growth.

DOI: 10.1103/PhysRevE.71.051606 PACS number(s): 81.10.Aj, 81.30.Fb

I. INTRODUCTION

Because of the tremendous importance of crystallization (e.g., in mineralization, materials manufacturing, and precipitation), crystallization front propagation has been modeled theoretically since the late 19th century [1,2]. Many of these studies examine the diffusion-limited propagation of a single domain from a molten or solvated state. One common approach is to treat crystallization as a Stefan problem in which local quasiequilibrium is maintained at the moving growth front while heat, impurities, or solvent excess generated at the front is carried away by diffusion [2,3].

In many cases of interest, competition between simultaneously crystallizing domains results in a complicated microstructure. For compact domains, the resulting microstructure exhibits grains with relatively simple shapes. Few theoretical studies have addressed the case where multiple domains with complicated front structures produce a solid with a complicated microstructure. This case is, however, relevant to many systems of interest, such as crystallization from solution, where solidification is incomplete, and crystallization of polymers, where the resulting structure consists of a noncrystalline arrangement of crystalline lamellae, which are often separated by amorphous material. One important example is spherulitic growth in which crystallites are arranged in a radial array bound by a spherical envelope which propagates at constant speed [4]. This morphology is typical of polymers, but is seen in other materials, usually at deep undercoolings, as well.

Here, we present a continuum model of network growth which considers solute diffusion and a simple treatment of growth kinetics. We apply our model to the crystallization of normal alkanes from solution in the presence of additives that affect the kinetics of growth. Pure *n*-alkanes typically crystallize as thin plates—often hundreds of micrometers across and only a few micrometers thick—due to large anisotropy in growth velocities for different crystallographic directions. Specific additives developed by the petroleum industry to prevent the precipitation of alkanes from diesel fuels and fuel oils at low temperatures cause alkanes to crystallize as a highly branched meshlike network. In a previous study, we reported the characteristics of such networks, including the formation of a distinctly banded structure when crystallized in a moving temperature gradient [5]. We find that our model is able to reproduce the essential behavior of the banded crystallization. We describe our experimental techniques and results in Secs. II and III, respectively, present our continuum growth model in Sec. IV, and compare the model results, obtained in Sec. V, with the experimental data.

II. EXPERIMENTAL METHODS

The experimental methods employed here have been previously reported [5]. Briefly, samples consisted of tricosane (n-$C_{23}H_{48}$, which we refer to as C_{23}) dissolved in dodecane (n-$C_{12}H_{26}$, or C_{12}), at concentrations of 18–55 mol %. To some of the samples was added a small amount (2% by mass for the studies reported here) of poly(octadecyl acrylate), hereafter referred to as PA-18, which is known to affect the kinetics of alkane crystallization [5,6].

For visualization by optical microscopy, sample cells consisting of square glass plates approximately 2 cm across separated by wire spacers of diameter 75 μm were filled with the sample solutions. The sample cells were sealed using an adhesive that crosslinks on exposure to UV radiation (NOA 61, Norland Products).

Crystallization of the samples was studied by video microscopy using an optical microscope (Olympus BX-60), video camera (Sony DXC-390), and frame grabber (Scion CG-7). The sample temperature was controlled by a directional solidification stage in which the sample is translated at a constant velocity through a known temperature gradient. Directional solidification allows the growth front to be examined at an approximately constant position in the laboratory frame.

*Permanent address: Dept. of Materials Science & Engineering, Tsinghua University, Beijing, China.
†Author to whom correspondence should be addressed. Electronic address: jhutter@uwo.ca

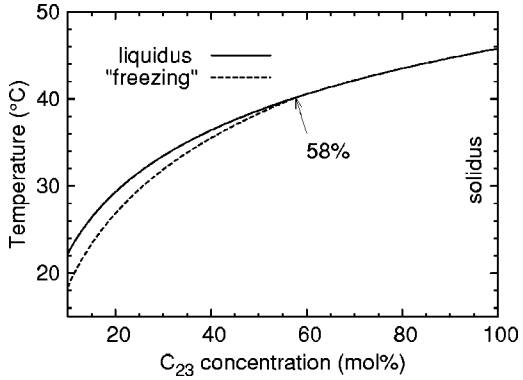

FIG. 1. Phase separation behavior of C_{23}/C_{12} solutions. The solvated state is unstable below the liquidus (solid curve), resulting in solidification of a nearly pure C_{23} phase. For small C_{23} concentrations ($\lesssim 58\%$), solidification typically begins at temperatures below the dashed curve, while no significant undercooling is seen at higher concentrations.

Data from the resulting growth movies were analyzed using custom macros created with digital image processing software (NIH Image, v. 1.61).

III. EXPERIMENTAL RESULTS

The phase behavior of this binary solution has been experimentally studied [7]. The phase diagram is somewhat complicated, with C_{23} able to solidify into an orthorhombic crystalline phase, or one of several "rotator" phases. Figure 1 summarizes the details required for our analysis. The solid curve indicates the liquidus curve, below which the solution phase separates into a C_{23} depleted solution and a solid C_{23} phase (e.g., crystalline or rotator). Since C_{12} is only sparingly soluble in the solid phases of C_{23}, the solidus line is vertical on the right edge of the graph. Experimentally, we have observed that for high C_{23} concentrations ($\gtrsim 58\%$), it is difficult to achieve significant undercooling before solidification begins [5]. At low concentrations, however, a reproducible degree of undercooling is achieved, as represented by the dashed curve in Fig. 1. This has been explained as the result of nucleation via a transient, metastable phase (with negligible nucleation barrier), which becomes possible at a *thermodynamically* determined undercooling [7].

Pure normal alkanes with odd chain length between 11 and 43 typically crystallize into the orthorhombic structure, forming platelike crystals with large {001} faces bound by {110} and {010} planes [8]. The [001] direction, corresponding to the orientation of the alkane molecules, is then the slow growth direction. In the presence of PA-18, the crystals instead form a meshlike, highly branched network. This growth morphology is illustrated in Fig. 2.

When crystallized by directional solidification, we find that for low imposed sample velocities ranging up to $\sim 6\ \mu$m/s, the crystallized network is organized into bands, as shown in Fig. 3. In most cases, successive bands nucleate *ahead* of the primary growth front and grow laterally to cover the previous band. This process repeats at approximately equal intervals, resulting in a nearly periodic pattern

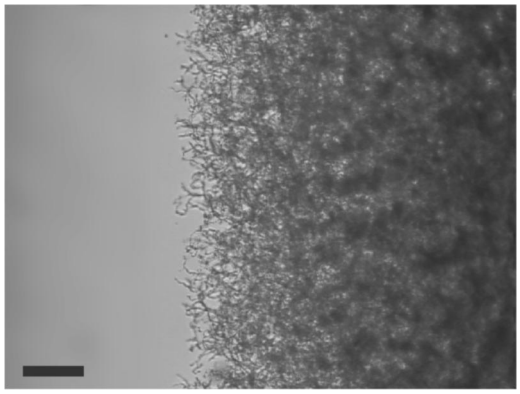

FIG. 2. Meshlike network formed by C_{23} crystallization from 34 mol % solution in C_{12} in the presence of 1.7×10^{-3} mol % PA-18. In this case the sample is moved to the right in a temperature gradient of 10 °C/mm at a constant velocity of 32 μm/s, resulting in a front that remains at a nearly constant location in the gradient. The scale bar is 100 μm.

of bands perpendicular to the sample motion. X-ray diffraction data (not shown) reveals no preferred orientation of crystallites relative to the imposed growth direction.

The lateral growth of a new band is quite rapid ($\sim 80\ \mu$m/s) relative to the average rate of advance of the front. As a result, the average front position advances in nearly steplike fashion controlled by the formation of new bands, with growth of the previous band playing only a minor role. However, the density of crystallites within a band continues to increase after the initial formation of the band, as evident in Figs. 3 and 4. Figure 4 shows the increase in optical density of two bands as a function of time.

We measured the dependence of the band repeat spacing on experimental parameters, such as the imposed velocity and C_{23} concentration. The results summarized in Fig. 5 [spacing vs (a) imposed velocity and (b) C_{23} concentration] indicate that the repeat spacing is a decreasing function of both parameters. Measurements of the dependence of the spacing on the temperature gradient (not shown) indicate that the spacing decreases with increasing gradient.

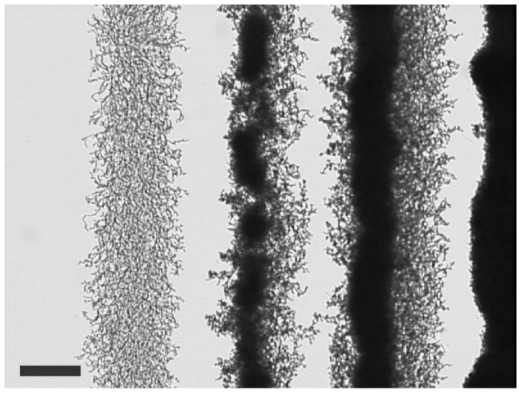

FIG. 3. Banded morphology resulting from directional solidification of C_{23} in the presence of 1.7×10^{-3} mol % PA-18. Here the C_{23} concentration was 34 mol %, and the imposed velocity was 1.6 μm/s. The scale bar measures 200 μm.

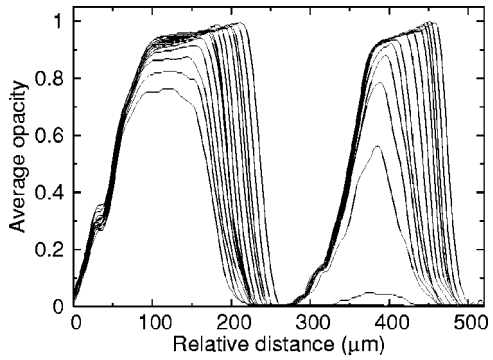

FIG. 4. Sample opacity (in arbitrary units) as a function of position in the sample averaged laterally in a direction perpendicular to the gradient. Fifteen profiles separated by 20 s intervals are shown for a sample of C_{23} concentration 34 mol % and PA-18 concentration 1.7×10^{-3} mol % as it is moved with a velocity of 3.2 μm/s through a gradient of 10 °C/mm.

IV. A CONTINUUM MODEL FOR MESH GROWTH

The experimentally motivated mathematical challenge is to develop a simple mesh growth model that can be applied to an isotropic disorganized clutter of fibrils. A few mesh growth models have been previously suggested, particularly for spherulitic growth. These models study mechanisms for lamellar branching [9], bundle formation [10], fibril alignment within a spherulite [11], and crystallization into macroscopic multispherulitic structures [12,13]. Several mathematical studies have been devoted to the surprising stability of spherulitic fronts [14]. The kinetically-limited aggregation regime has been modeled by cellular automata [15], which were subsequently approximated by two coupled partial differential equations [16]; however, these models were developed for radial growth and with a single fixed growth direction, and so may not be applied to our system.

We choose to model the growth in a coarse-grained approximation, where volumes of interest are far larger than any individual crystal or structural unit. Formulated as such, our model does not predict the formation of the network geometry itself, but is powerful enough to describe propagation of the crystallization front and thickening due to continuing crystallization in regions left behind. We consider the volume fraction of crystals $\phi(\mathbf{x},t)$ to be the only important field variable of the aggregate, with mesh geometry factors included via predefined constants that can be estimated from experimental data. In Sec. IV A, we develop a partial differential equation, similar to the Fisher-Kolmogorov-Petrovsky-Piskunov (FKPP) equation, to describe the growth. The FKPP equation, presented in 1937 [17], and variants have been successfully applied to various processes involving nonlinear front propagation, including crystallization [1]. An extensive review of the classical FKPP equation can be found in Ref. [18].

The growth-evolution equation alone is not sufficient to explain the banding process. Observations that nucleation events persistently occur ahead of the front, but not in the cooler region closer, can be explained by solute depletion (and consequent decreased supersaturation) at the growing front. The width of the depletion zone is expected to be $\sim D/v_f$, where D is the diffusion constant and v_f is the front velocity. This expected width is of the same order of magnitude as the observed band spacings. Beginning with empirical laws for diffusion in porous media in Sec. IV B, we include mass transfer via a second partial differential equation.

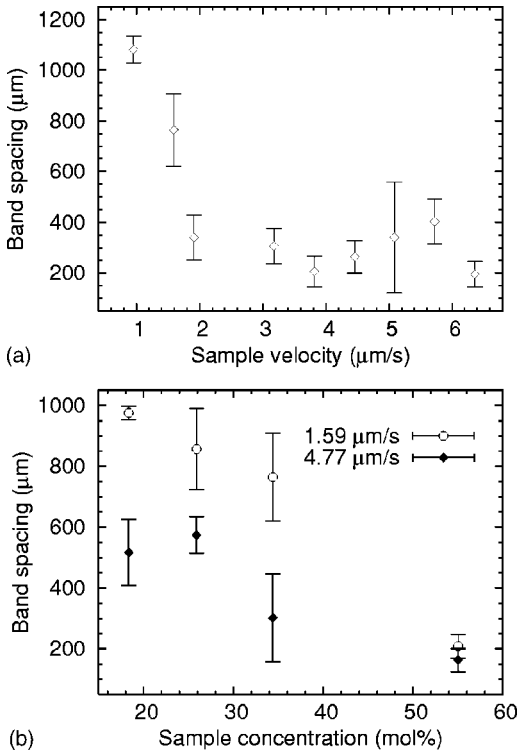

FIG. 5. Band repeat spacing as a function of (a) imposed velocity for a sample of concentration of 34 mol %, and (b) C_{23} concentration for two different imposed velocities. The temperature gradient was 10 °C/mm in both cases. (Adapted from [5].)

A. Growth-evolution equation

In order to develop the continuum approximation, we formally separate the growing aggregate into aggregation units. Each aggregation unit has the same volume ν, the same number of faces n^j of each type j, and the same dimensions l^j, measured perpendicular to the faces. The units are assumed to occupy the same volume whether they are aggregated or diffusing in solution.

The time evolution of ϕ depends, in general, on two types of terms, representing local and nonlocal effects. The local-growth terms cause "thickening" of the structure. The nonlocal, gradient terms allow the structure to propagate in space.

Let us begin by considering the homogeneous case. If a face of type j grows (by one aggregation unit) with probability p_t^j per unit time, the growth rate of the crystalline volume fraction ϕ is approximately

$$\frac{\partial\phi}{\partial t} = \nu\sum_j s^j p_t^j, \tag{1}$$

where s^j is the number of faces of type j per unit volume available for growth (which we refer to as open faces). The

growth probability per unit of time of a face j can be estimated as the ratio of its normal growth velocity v^j to the aggregation unit dimension l^j. The densities of open crystalline faces s^j, are possibly very complicated, model dependent functions involving the microstructure of the aggregate. In general, the functions should initially increase with increasing crystalline volume fraction, later start to decrease and eventually approach zero when little uncrystallized space is available. As an approximation, we assume that the open face densities are approximately equal to the product of the number of units per volume ϕ/ν, number of faces n^j of type j on an isolated growth unit, and the probability $(1-\phi)$ that there is no other aggregation unit located next to the unit's face. Consequently, $s^j = n^j \phi(1-\phi)/\nu$; this is also the simplest function that has the correct mathematical behavior. In assuming that all faces have an equal probability of being open, we are ignoring details of the microstructure. Since we expect individual branches to be randomly distributed, the closer l^j is to actual structural measurements such as the distance between branching points, branch thickness, etc., the better one would expect the estimate to work. The approximation leads to

$$\frac{\partial \phi}{\partial t} = \phi(1-\phi)\sum_j \alpha^j v^j, \tag{2}$$

where the mesh geometry factors $\alpha^j = n^j/l^j$ can be estimated from experimental data.

Equation (2) can be extended to branched networks if we allow n^j to be fractional. Formally,

$$n^j = n_0^j\left(1 + \sum_{k=2}(k-1)p_k^j\right), \tag{3}$$

where n_0^j is actual number of faces of type j on one unit and p_k^j is the probability that a face j branches into k units when it grows.

Next we consider nonuniform growth. Let us consider a small volume inside of the large sample. If the aggregate is not spatially uniform, we must account for an imbalance between the number of crystals growing in both directions across the surfaces of this volume. This can be done as a sum over the growth faces j and growth directions. We divide the volume further into elementary slices by coordinate surfaces perpendicular to one of the basis vectors $\hat{\mathbf{e}}_1$ (see Fig. 6). We choose each elementary slice to have thickness $l^j = h_1 dx_1$ and volume $l^j h_2 h_3 dx_2 dx_3$, where the h_i are scale factors. First, we account for aggregation units growing into the slice centered at x_1 from the left. The slice on the left contains $[l^j h_2 h_3 dx_2 dx_3] n^j \phi(x_1 - dx_1)/\nu$ faces of type j, of which a fraction η_{1+}^j are oriented in the $\hat{\mathbf{e}}_1$ direction. These faces grow with a probability per unit time v^j/l^j, each increasing the crystallized volume by ν per growth event. The crystals that cross the boundary into the selected slice are limited by the available space in that slice, and not in their slice of origin. Thus, the growth is "unblocked" with probability $1-\phi(x_1)$. Because of the choice of slice thickness, only half of the generated volume, on average, crosses the slice border. Similarly, we must subtract the solid volume that would have been grown inside of the slice, but instead escaped through the left surface. Therefore, the net correction to the grown volume due to the left surface alone is

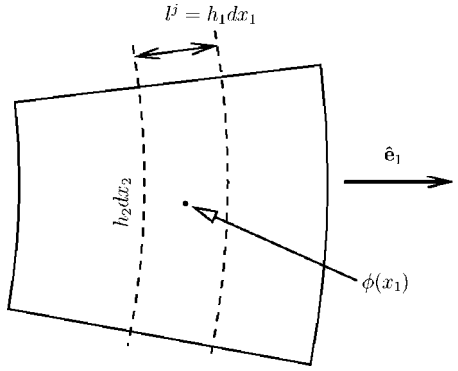

FIG. 6. Schematic of an elementary slice defining the variables used in the text.

$$[l^j h_2 h_3 dx_2 dx_3]\frac{n^j}{\nu}[\phi(x_1 - dx_1)\eta_{1+}^j - \phi(x_1)\eta_{1-}^j]$$

$$\times [1-\phi(x_1)]\frac{v^j}{l^j}\frac{\nu}{2}. \tag{4}$$

If we assume that the fraction of all (open and blocked) j faces oriented in the $\hat{\mathbf{e}}_i$ direction is equal to the fraction of all j faces oriented in the $(-\hat{\mathbf{e}}_i)$ direction (i.e., $\eta_{i+}^j = \eta_{i-}^j = \eta_i^j$), this correction becomes

$$-\frac{1}{2}dx_2 dx_3 n^j v^j [1-\phi(x_1)]\left[h_2 h_3 \frac{\eta_1^j}{h_1}\frac{\partial \phi}{\partial x_1}\right]_{x_1 - dx_1/2}. \tag{5}$$

When we add the similar correction for growth across the right surface,

$$\frac{1}{2}dx_2 dx_3 n^j v^j [1-\phi(x_1)]\left[h_2 h_3 \frac{\eta_1^j}{h_1}\frac{\partial \phi}{\partial x_1}\right]_{x_1 + dx_1/2}, \tag{6}$$

replace the difference by a derivative, and divide by the slice volume $l^j h_2 h_3 dx_2 dx_3$, we obtain the correction to $\partial\phi/\partial t$ due to faces j and direction $\hat{\mathbf{e}}_1$,

$$[1-\phi(x_1)]\kappa^j v^j \frac{1}{h_1 h_2 h_3}\frac{\partial}{\partial x_1}\left[h_2 h_3 \frac{\eta_1^j}{h_1}\frac{\partial \phi}{\partial x_1}\right], \tag{7}$$

where $\kappa^j = n^j l^j/2$.

This correction procedure must be repeated for all face types j and directions $\hat{\mathbf{e}}_i$. Summation over j and i leads us to the final growth evolution equation

$$\frac{\partial \phi}{\partial t} = (1-\phi)\sum_j v^j[\alpha^j \phi + \kappa^j \nabla(\tilde{\eta}^j \nabla \phi)], \tag{8}$$

where $\tilde{\eta}^j$ is the set of diagonal matrices $\mathrm{diag}(\eta_1^j, \eta_2^j, \eta_3^j)$, representing the distribution of faces of type j over the three orientations.

In cases that are purely kinetically limited, the normal growth velocities $v^j(c,T)$ are parameters. Otherwise, they are functions of the unknown fields, to be determined by including mass and heat transfer equations.

B. Mass transfer equation

Growing branches of the aggregate present obstacles to the path of the diffusing molecules, decreasing diffusion rates. Diffusion in such media is a mathematically complicated problem. Therefore, either of two semiphenomenological treatments are typically used [19,20]. Both approaches adjust the diffusion constant D in Fick's law,

$$\mathbf{J}_c = -D\,\boldsymbol{\nabla} c, \tag{9}$$

where c is a concentration in moles per volume and $\mathbf{J}_c$ is the corresponding current density. The first approach to adjust D is to multiply the diffusion constant in homogeneous solution, D_0, by porosity of the structure $(1-\phi)$ divided by tortuosity (a path complexity parameter). The other approach, adopted here, is to include the phenomenology into one multiplier $(1-\phi)^m$. The exponent m has been estimated for different media and found to be close to 2 [19]. We thus assume an effective diffusion constant given by

$$D(\phi) = D_0(1-\phi)^2. \tag{10}$$

Considering mechanical flows makes the problem needlessly complicated, hence we assume that there is no volume change during crystallization. This assumption is formally equivalent to the claim that an aggregation unit occupies the same volume in both the crystal and liquid phases. Mass transport by aggregation unit diffusion must also satisfy local mass conservation:

$$\frac{\partial \rho}{\partial t} = -\,\boldsymbol{\nabla}\cdot\mathbf{J}_c, \tag{11}$$

where ρ is the total molar density of the aggregate material (including aggregation units in both the solid and liquid phases). If we incorporate Eq. (9) into Eq. (11) and multiply by the molar volume of the solute, we can express the mass transfer equation in terms of volume fractions:

$$\frac{\partial \psi}{\partial t} = \boldsymbol{\nabla}\cdot(D\,\boldsymbol{\nabla} w), \tag{12}$$

where w is the volume fraction of solvated material in the liquid phase, and ψ is the total volume fraction of the material (including both the phases). Since w and ψ are related via $w=(\psi-\phi)/(1-\phi)$, the mass transfer equation can be expressed as

$$\frac{\partial \psi}{\partial t} = D_0[(1-\phi)\nabla^2\psi - (1-\psi)\nabla^2\phi]. \tag{13}$$

V. MODEL RESULTS

The system of equations described in the previous section can be readily used to model front propagation of an aggregate. As a demonstration, we use it to model the aggregate bands described in Sec. III. In this section, we justify our choice of parameters and present the results of numerical solutions to Eqs. (8) and (13) in the one-dimensional case appropriate to directional solidification.

From optical microscopy data, we estimate the width of the crystalline branches to be $\sim 1\ \mu$m. As an approximation, the aggregation units are assumed to be cubes, so $l^j = 1\ \mu$m for all j. In keeping with the network structure, we assume that the cubes have two types of faces. Two opposite faces, type 1, can either grow with rate v^1 or branch with probability ~ 0.1. The other four faces, type 2, are assumed to be quickly inhibited, so that their effective growth rates are taken to be zero: $v^2 = 0$. In the case of anisotropic structures, such as those observed in spherulites, one may need to use unequal diagonal values in the face orientation matrices $\mathrm{diag}(\eta_r^j, \eta_\theta^j, \eta_\varphi^j)$, e.g., $\eta_r^j \neq \eta_\varphi^j$. In the case of the banding problem considered here, we adopt an isotropic face orientation distribution where $\eta_i^1 = 1/6$. Thus Eq. (8) simplifies to

$$\frac{\partial \phi}{\partial t} = v(1-\phi)[\alpha\phi + \kappa\nabla^2\phi], \tag{14}$$

where $\kappa \sim 1/\alpha \approx 1\ \mu$m. We neglect the branching probability and the orientation matrices at this point due to the rough estimates of α and κ.

The most difficult quantity to estimate for this model is the growth rate v. For simple growth mechanisms, the growth rate is a power of the chemical potential difference $\Delta\mu$ between the solid and liquid phases, where the power law depends on the details of the growth mechanism. In the presence of the kinetic inhibitor, the growth rate does not obey such a simple growth law. As an approximation, we use a generic case of $v \propto c_{eq}\Delta\mu$ [3], where c_{eq} is the equilibrium molar fraction in the solution, and $\Delta\mu = k_B T \ln(c/c_{eq}) \approx k_B T(c/c_{eq} - 1)$. Consequently, we use

$$v = v_k(c - c_{eq}), \tag{15}$$

where $v_k \approx 5\times 10^{-6}$ m/s is chosen so that v at the instant of nucleation agrees with the experimentally measured lateral growth velocities. The equilibrium concentration c_{eq} is determined from a fit to the experimental liquidus curve [5,7] according to

$$T(c_{eq}) = a_X + b_X \ln(c_{eq}), \tag{16}$$

where $a_X = 45.9\ ^\circ$C and $b_X = 10.2\ ^\circ$C. In the conserved volume approximation, molar fraction c is related to volume fraction in the solution w by $1/c - 1 = \lambda(1/w - 1)$, where λ is the solvent to solute molar volume ratio.

As discussed above, new bands are initiated by nucleation events ahead of the front; consequently, a nucleation term $\nu^* J_0$, where ν^* is the volume of the critical nucleus, and J_0 is the nucleation rate, must be introduced into Eq. (14). Then

$$\frac{\partial \phi}{\partial t} = v(1-\phi)[\alpha\phi + \kappa\nabla^2\phi] + \nu^* J_0. \tag{17}$$

Since the nucleation events reproducibly occur at undercoolings defined by the "freezing" or "rotator" curve, we approximate the nucleation term via a step function as

$$\nu^* J_0 = \nu_0 H(c - c_R(T)), \tag{18}$$

where H is Heaviside step function, $c_R(T)$ is the rotator curve (i.e., the reproducible freezing curve), and ν_0 is a nucleation seed. We found nearly identical results for a broad range of small values of ν_0. The rotator curve was also measured [5,7] and found to be

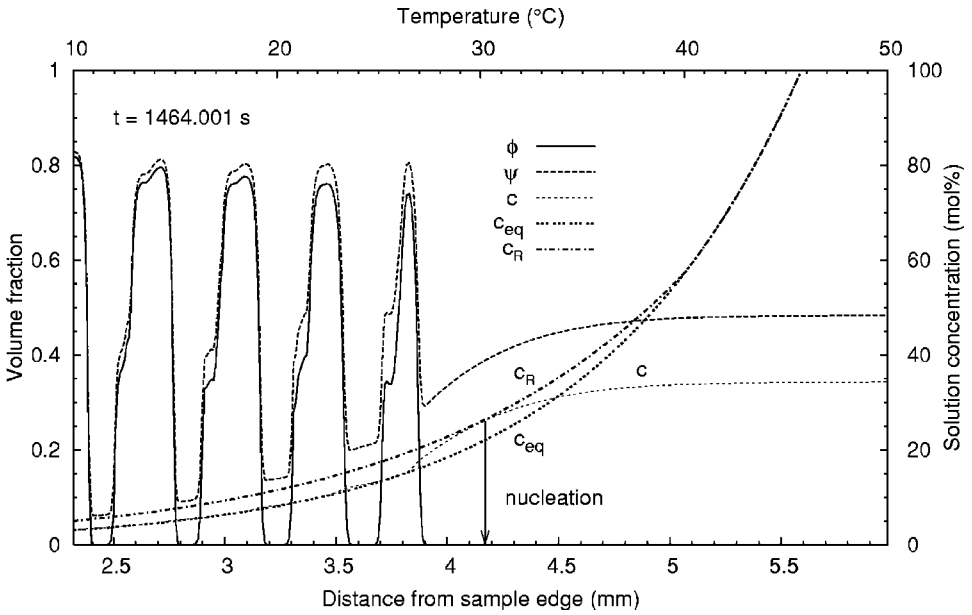

FIG. 7. Snapshot of the simulated evolution of the banded network showing crystallized fraction and solute concentration relative to the phase diagram. ϕ and ψ are in terms of volume fraction, while c, the liquidus curve c_{eq}, and the freezing curve c_R are measured in mol %. In this case, the C_{23} concentration was 34 mol % and imposed velocity was 1.6 μm/s.

$$T(c_R) = a_R + b_R \ln(c_R) + c_R \ln^2(c_R), \tag{19}$$

where a_R=47.24 °C, b_R=13.0 °C, and c_R=0.19 °C.

The temperature gradient in the sample is imposed by temperatures of 10 and 50 °C maintained at opposite sides of a 3.7 mm gap. The temperature inside of the ~0.075 mm thick sample is nearly identical to the temperature of the ~1.3 mm thick enclosing glass. When the sample is moved with a constant velocity from the hot to cold side of the apparatus, the gradient is not constant throughout the sample, due to the finite heat conductivity of glass. The deviation is easy to estimate theoretically by solving the heat conductivity equation in the lab frame (which is moving with respect to the glass). The maximum deviation expected is 0.6%. Therefore, the temperature gradient can be considered constant throughout the sample.

The diffusion constant for C_{23} in C_{12} is estimated to be $D_0 \approx 5 \times 10^{-6}$ cm^2/s, based on results of Ref. [21].

Using the boundary conditions

$$(\nabla \phi)_n = 0 \text{ and } (\nabla \psi)_n = 0 \tag{20}$$

guarantees zero mass current through sample borders.

We solve the system of Eqs. (13), (17), and (20) with a parallel implementation of the explicit finite difference method [22], using Message Passing Interface (MPI) [23].

Our model produces the distinct banded structures for a range of imposed velocities. Figure 7 represents the gradient portion of the sample in the banded growth regime. In the particular frame shown, a new band has just nucleated: the solution concentration curve is nearly tangent to the freezing (rotator) curve at the nucleation point. A series of frames, as shown in Fig. 8, shows the evolution of a pair of bands. Of note are the observations that growth of a band occurs predominantly on the warm side, and that growth continues after nucleation of the next band. We performed a series of runs at varying imposed sample velocities and initial C_{23} concentrations to determine the dependence of the band repeat spacing on sample conditions for our model. The results are shown in Fig. 9. As can be seen, the band spacing decreases with increasing imposed velocity and increasing concentration.

VI. DISCUSSION

Our simulations of directional solidification based on the model described in Sec. IV exhibit the same behavior as we observed in the experimental studies described in Sec. III. In particular, including the possibility of nucleation results in the formation of a banded structure. To generate this simulation data, we assume that nucleation occurs reproducibly at the instant when the rotator phase becomes stable relative to the solution phase, even though it is not stable relative to the crystalline phase. This nucleation mechanism via a metastable phase has been previously invoked to explain the reproducible freezing temperature observed for alkane solutions [7]; here, it results in the regular nucleation of new bands in the supersaturated region ahead of the growth front.

Both experimental and numerical results show that the bands grow predominantly on their warmer edges, presumably because of depletion due to growth of the previous

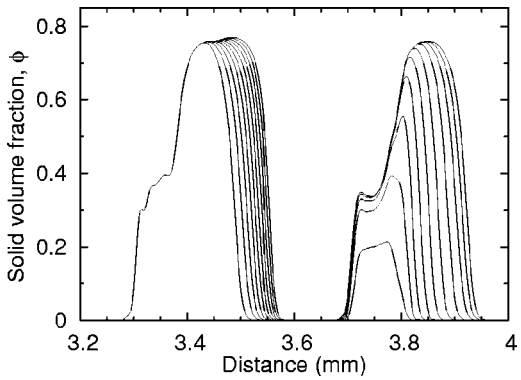

FIG. 8. Volume fraction of solid phase. Ten profiles separated by 40 s intervals are shown for the same simulation as in Fig. 7.

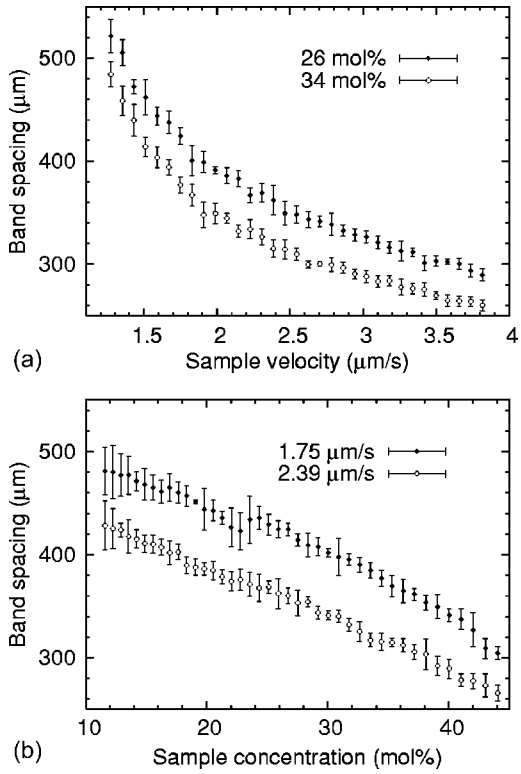

FIG. 9. Band repeat spacing as a function of sample velocity (a) and sample concentration (b). Error bars represent 95% confidence intervals due to statistical variation of the spacing during one simulation run.

band. The details of the profile shapes depend on the growth conditions in both the experimental and numerical cases. The model predicts a dependence of the spacial period of the bands on parameters such as imposed velocity and initial solution concentration that is in agreement with the experimental findings. Such agreement between model and experiment strongly suggests that the mechanism for band formation initially presented in [5] is essentially correct.

Although the solute concentration considered here is much higher than that of any single component in a typical diesel fuel or fuel oil, the possibility of nucleation and growth via the rotator phase may be an important consideration in the development of improved additives for low-temperature operability. For instance, this mechanism may allow growth of new crystals even when existing crystals have been completely inhibited. Alternatively, deliberately exploiting this nucleation mechanism may allow the generation of an increased number of crystal nuclei, resulting in smaller crystals for a given crystallized fraction.

Curiously, our experimental results do not show a strong dependence of the *lateral* growth velocity on imposed velocity (though it does depend weakly on the initial sample concentration with lower lateral velocities for higher concentrations). This implies that the supersaturation of the crystalline phase at the time of band nucleation is relatively constant regardless of the band spacing. The numerical results also show an approximately constant supersaturation at the instant of nucleation over a broad range of sample velocities. This can be understood in terms of Fig. 7, which shows that the separation of the curves c_R and c_{eq} in the temperature gradient remains approximately constant over a wide range.

The velocity ranges studied are limited at the low end for the same reason in both the experimental and numerical cases: finite sample size. Too few bands can form in a sample after initial transient effects and before the approaching sample boundary becomes important. At higher velocities, the experimental bands do not form clean parallel structures and eventually merge. The bands produced by the model also become indistinguishable at higher imposed velocities.

Although the model presented here was developed to describe a particular crystallization system, it may be possible to apply it to a larger variety of crystallization processes involving a nondense front of crystallites. One of its key features is that it considers both growth kinetics and diffusion, unlike, e.g., the Stefan model, in which equilibrium (or small departures from equilibrium) is assumed at the front [1]. This was necessary for a description of our experimental system, in which both processes are important. Growth immediately after nucleation is in a strongly supersaturated (and therefore kinetics-limited) regime, as evident from observations of an initially spherulitic morphology [5]. Diffusion becomes important during the later stages of growth, when the supersaturation decreases and depletion results in a nearly complete cessation of growth on the trailing edges of bands. The ability to include both kinetics- and diffusion-limited growth will also be useful in cases where a crossover can occur due to changing crystallization conditions.

Our model is easily applied to cases with cylindrical and spherical symmetry. In these cases, our numerical results (not shown) indicate a constant front velocity in the isothermal case appropriate to spherulitic growth [24]. While other models have been proposed to describe such cases, they involve a detailed description of the microstructure (including, for instance, a radial orientation of crystallites), which varies from system to system and is not always well characterized. Although results which depend on such details are lost in our model, an understanding of the essential behavior on larger length scales is often the principal goal.

VII. CONCLUSIONS

We have described a simple model for the growth of crystalline networks from solution. This model incorporates solute diffusion, realistic kinetics based on the thermodynamic phase diagram, and parameters that can be obtained from independent experiments. While the model invokes several approximations (for instance, the microscopic structure of the network is assumed rather than predicted, and the dependence of the growth on the details of the structure is only considered in a mean-field sense), it is able to capture the essential features of growth of a crystalline network.

We have used this model to understand the formation of a unique banded crystallization structure reported in an earlier work. The model exhibits the main features of the banded growth, is able to predict the correct dependence of the band spacing on several experimental parameters, and produces a

band density-profile evolution in qualitative agreement with the experimental observations.

In addition to its value in modeling the specific crystallization system studied here, we expect that this model, particularly in its two- and three-dimensional invocations, may be useful for understanding other crystalline networks with meshlike fronts.

ACKNOWLEDGMENTS

This work was funded by NSERC (Canada) and by the Imperial Oil Charitable Foundation. One of the authors (J.Z.) would also like to thank the Centre for Chemical Physics at UWO for financial support. We also gratefully acknowledge helpful discussions with Ivan L'Heureux.

[1] *Solids Far from Equilibrium*, edited C. Godrèche (Cambridge University Press, Cambridge, England, 1992).
[2] V. Alexiades and A. D. Solomon, *Mathematical Modeling of Melting and Freezing Processes* (Hemisphere, Washington, 1993).
[3] Y. Saito, *Statistical Physics of Crystal Growth* (World Scientific, Singapore, 1996).
[4] P. J. Phillips, in *Handbook of Crystal Growth*, edited by D. T. J. Hurle (North-Holland, Amsterdam, 1993), Vol. 2b, Chap. 18, pp. 1167–1216.
[5] J. L. Hutter *et al.*, J. Cryst. Growth **273**, 292 (2004).
[6] A. J. Colussi, M. R. Hoffmann, and Y. Tang, Langmuir **16**, 2405 (2000); D. H. M. Beiny, J. W. Mullin, and K. Lewtas, J. Cryst. Growth **102**, 801 (1990); R. Kern and R. Dassonville, *ibid.* **116**, 191 (1992); X. Ding, G. Qi, and S. Yang, Polymer **40**, 4139 (1999).
[7] E. B. Sirota, J. Chem. Phys. **112**, 492 (2000).
[8] P. Bennema, in *Handbook of Crystal Growth*, edited by D. T. J. Hurle (North-Holland, Amsterdam, 1993), Vol. 1a, Chap. 7, pp. 545–571.
[9] N. Goldenfeld, J. Cryst. Growth **84**, 601 (1987); E. Ben-Jacob *et al.*, Phys. Rev. Lett. **57**, 1903 (1986).
[10] K. M. Kit and J. M. Scholtz, J. Polym. Sci., Part B: Polym. Phys. **36**, 873 (1998).
[11] S. Swaminarayan and C. Charbon, Polym. Eng. Sci. **38**, 634 (1998).
[12] C. Charbon and S. Swaminarayan, Polym. Eng. Sci. **38**, 644 (1998).
[13] V. Capasso, M. Burger, A. Micheletti, and C. Salani, in *Mathematical Modelling for Polymer Processing*, edited by V. Capasso (Springer-Verlag, Berlin, 2003), Chap. 5, pp. 167–242.
[14] A. Gadomski and J. Łuczka, Int. J. Quantum Chem. **52**, 301 (1994); B. Caroli, C. Caroli, B. Roulet, and G. Faivre, J. Cryst. Growth **94**, 253 (1989); J. K. Lin and D. G. Grier, Phys. Rev. E **54**, 2690 (1996).
[15] L. D. Sander, Contemp. Phys. **41**, 203 (2000); P. Meakin, *Fractals, Scaling and Growth far from Equilibrium* (Cambridge University Press, Cambridge, England, 1998).
[16] J. Los *et al.*, J. Phys.: Condens. Matter **12**, 3195 (2000).
[17] R. A. Fisher, Annals of Eugenics **7**, 353 (1937); A. Kolmogorov, I. Petrovsky, and N. Piskunov, Moscow University Bulletin of Mathematics **1**, 1 (1937).
[18] J. D. Murray, *Mathematical Biology* (Springer-Verlag, New York, 1989), Chap. 11, pp. 277–310.
[19] P. Grathwohl, *Diffusion in Natural Porous Media: Contaminant Transport, Sorption/Desorption and Dissolution Kinetics* (Kluwer Academic Publishers, Boston, 1998).
[20] B. E. Logan, *Environmental Transport Processes* (John Wiley and Sons, New York, 1999).
[21] W. Hayduk and B. S. Minhas, Can. J. Chem. Eng. **60**, 295 (1982).
[22] W. F. Ames, *Numerical Methods for Partial Differential Equations*, 3rd ed. (Academic Press, Boston, 1992).
[23] H. El-Rewini and T. G. Lewis, *Distributed and Parallel Computing* (Manning Publications, Greenwich, 1997).
[24] Spherulites also are known to exhibit banded patterns. Such patterns are related to the orientation of crystallites and are not related to periodic density variations studied here; see, e.g., D. Patel and D. Bassett, Polymer **43**, 3795 (2002); J. L. Hutter and J. Bechhoefer, J. Cryst. Growth **217**, 332 (2000).